

Cobalt(II) Coordination Polymers Assembled from Unexplored Pyridine-Carboxylic Acids: Structural Diversity and Catalytic Oxidation of Alcohols

Jinzhong Gu,^{*,†} Min Wen,[†] Yan Cai,[†] Zifa Shi,[†] Dmytro S. Nesterov,[‡] Marina V. Kirillova,[‡] and Alexander M. Kirillov^{*,‡,§}

[†]State Key Laboratory of Applied Organic Chemistry, Key Laboratory of Nonferrous Metal Chemistry and Resources Utilization of Gansu Province, College of Chemistry and Chemical Engineering, Lanzhou University, Lanzhou 730000, People's Republic of China

[‡]Centro de Química Estrutural, Instituto Superior Técnico, Universidade de Lisboa, Av. Rovisco Pais, 1049-001, Lisbon, Portugal

[§]Peoples' Friendship University of Russia (RUDN University), 6 Miklukho-Maklaya st., Moscow, 117198, Russian Federation

Supporting Information

ABSTRACT: New coordination polymers of cobalt(II), namely, $[\text{Co}(\mu_4\text{-cpna})(\text{H}_2\text{O})_2]_n$ (**1**), $[\text{Co}(\mu_3\text{-cpna})(\text{phen})(\text{H}_2\text{O})]_n \cdot n\text{H}_2\text{O}$ (**2**), $[\text{Co}_3(\mu_4\text{-dppa})_2(\text{H}_2\text{O})_6]_n \cdot 2n\text{H}_2\text{O}$ (**3**), and $[\text{Co}_3(\mu_5\text{-dppa})_2(\mu\text{-}4,4'\text{-bipy})(\text{H}_2\text{O})_2]_n \cdot 4n\text{H}_2\text{O}$ (**4**), have been generated under hydrothermal conditions from $\text{CoCl}_2 \cdot 6\text{H}_2\text{O}$, two different multifunctional pyridine-carboxylic acids { H_2cpna : 5-(4-carboxyphenoxy)nicotinic acid; H_3dppa : 5-(3,4-dicarboxylphenyl)picolinic acid}, and optional *N,N*-supporting ligands {phen: 1,10-phenanthroline; 4,4'-bipy: 4,4'-bipyridine} acting as mediators of crystallization. These Co(II) coordination polymers (CPs) have been obtained as stable crystalline materials and characterized by conventional solid-state techniques, including X-ray crystallography. The obtained products are 3D metal–organic frameworks (MOFs **1** and **4**) or 2D coordination polymers (CPs **2** and **3**). Analysis of the topologies of simplified nets has revealed the *sra* (**1**), *fes* (**2**), and 3,4L13 (**3**) networks, in addition to a very complex topologically unique framework in **4**. An observed diversity of structures is driven by types of carboxylate building blocks and crystallization mediators. Thermal stability and magnetic and catalytic properties of **1–4** have also been studied. In fact, the Co(II) compounds act as heterogeneous catalysts for the oxidation of alcohols with *t*BuOOH (*tert*-butylhydroperoxide) under mild conditions. Compound **2** features a good catalytic activity (up to 45% yield) in the oxidation of 1-indanol to 1-indanone. Finally, products **1–4** broaden a still very small number of CPs or MOFs driven by the present type of multifunctional pyridine-carboxylic acids (H_2cpna , H_3dppa).



INTRODUCTION

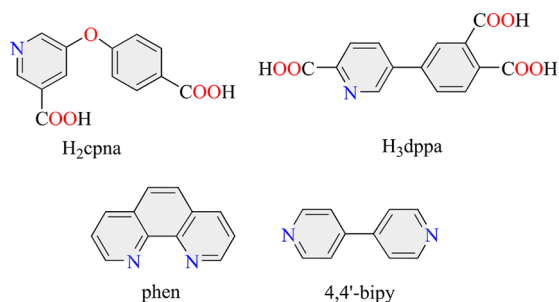
Design and synthesis of new coordination polymers and metal–organic frameworks (abbr. CPs and MOFs, respectively) has recently attracted an enormous attention due to an unlimited diversity of their structural types, architectures, topologies, as well as important properties and applications of these functional solids.^{1–10} In particular, the use of CPs in catalysis became a recognized research area,^{11–15} which is primarily associated with the high porosity, crystallinity, inorganic–organic hybrid structures, thermal stability, and tunable physicochemical properties of such compounds.^{11–15}

Among the vast variety of metal–complex and coordination polymer catalysts, coordination compounds that incorporate cobalt nodes and carboxylate blocks as spacers or linkers have deserved a special attention in catalysis.^{16–19} In fact, cobalt coordination compounds can catalyze a wide range of organic reactions, which span from C–H activation and cross-coupling to CO_2 reduction and water oxidation.^{20–23} Although many of these processes can be efficiently promoted by the platinum group complexes as catalysts, the first-row transition metals

such as cobalt are more abundant and less expensive, and thus can be of significant practical importance. In particular, some cobalt compounds with the ligands containing pyridyl and carboxylate functional groups catalyze the oxidation of alcohols and amines with peroxides or dioxygen.^{24–26}

By combining our recent research directions in the areas of (i) hydrothermal synthesis of functional coordination polymers^{27–30} and (ii) oxidation catalysis,^{31–33} herein we focused our attention on two poorly explored pyridine-(di/tri)-carboxylic acids (Scheme 1), namely, H_2cpna (5-(4-carboxyphenoxy)nicotinic acid) and H_3dppa (5-(3,4-dicarboxylphenyl)picolinic acid).^{27,34–39} Along with optional *N,N*-type mediators of crystallization (co-ligands), these carboxylic acids were probed as main organic blocks (Scheme 1) for hydrothermal synthesis of new cobalt(II) CPs. Besides, considering that these ligands (H_2cpna and H_3dppa) comprise two types of principal functional groups (pyridine and

Received: January 24, 2019

Scheme 1. Main Pyridine-Carboxylic Acid Ligands and *N,N*-Donor Crystallization Mediators

carboxylate), it was also interesting to investigate the catalytic behavior of respective cobalt(II) compounds toward the oxidation of alcohols.

Thus, the present study describes the hydrothermal preparation, crystal structures, characterization, thermal behavior, magnetic properties, as well as catalytic activity of a new series of cobalt(II) CPs and MOFs, namely, $[\text{Co}(\mu_4\text{-cpna})(\text{H}_2\text{O})_2]_n$ (**1**), $[\text{Co}(\mu_3\text{-cpna})(\text{phen})(\text{H}_2\text{O})]_n \cdot n\text{H}_2\text{O}$ (**2**), $[\text{Co}_3(\mu_4\text{-dppa})_2(\text{H}_2\text{O})_6]_n \cdot 2n\text{H}_2\text{O}$ (**3**), and $[\text{Co}_3(\mu_5\text{-dppa})_2(\mu\text{-4,4'-bipy})(\text{H}_2\text{O})_2]_n \cdot 4n\text{H}_2\text{O}$ (**4**). The obtained compounds represent the very rare (**1**, **2**) or unique (**3**, **4**) examples of cobalt(II) CPs derived from H_2cpna or H_3dppa , as confirmed by searching the Cambridge Structural Database (CSD).

EXPERIMENTAL SECTION

Reagents and Equipment. All chemicals and solvents (A.R. grade) were furnished by commercial suppliers. Elemental content (C, H, N) in **1–4** was studied on an Elementar Vario EL elemental analyzer. TGA (thermogravimetric analysis) data were collected on a LINSEIS STA PT1600 thermal analyzer (flow of N_2 , $10^\circ\text{C}/\text{min}$ heating rate). A Bruker EQUINOX 55 spectrometer was used to record the IR spectra (KBr discs). PXRD (powder X-ray diffraction) patterns were measured on a Rigaku-Dmax 2400 diffractometer ($\lambda = 1.54060 \text{ \AA}$ Cu $K\alpha$ radiation). Magnetic measurements were performed with a Quantum Design SQUID Magnetometer (MPMS

XL-7 model, field strength of 0.1 T) at 2–300 K; diamagnetic contribution was corrected before analyzing the data. Catalytic oxidation of alcohols was monitored by GC (gas chromatography) analyses that were carried out on an Agilent Technologies 7820 A chromatograph using a flame ionization detector, capillary column (BP20/SGE), and helium as a carrier gas.

Synthesis and Characterization of **1–4.** $[\text{Co}(\mu_4\text{-cpna})(\text{H}_2\text{O})_2]_n$ (**1**). $\text{CoCl}_2 \cdot 6\text{H}_2\text{O}$ (0.3 mmol, 71.0 mg), H_2cpna (0.3 mmol, 77.7 mg), NaOH (0.6 mmol, 24.0 mg), and H_2O (10 mL) were combined in a stainless steel (Teflon-lined) reactor of the 25 mL capacity. After vigorous stirring for 15 min at ambient temperature, a reactor was closed and kept at 160°C for 3 days in the oven. Then, the reactor was gradually cooled down ($10^\circ\text{C}/\text{h}$) to ambient temperature and opened. Yellow crystals (needles) were removed from the reaction mixture manually or by filtration, washed with H_2O , and then air-dried to furnish **1**. Yield: 65%, based on H_2cpna . Analysis calculated for $\text{C}_{13}\text{H}_{11}\text{CoNO}_7$: C 44.34, H 3.15, N 3.98%. Found: C 44.67, H 3.13, N 4.01%. IR (cm^{-1}): 3596w, 3068w, 1628s, 1596s, 1544m, 1499w, 1453w, 1401s, 1335s, 1297m, 1244w, 1206w, 1160w, 1095w, 1049w, 1003w, 958w, 918w, 860w, 821w, 770m, 699w, 652w, 554w.

$[\text{Co}(\mu_3\text{-cpna})(\text{phen})(\text{H}_2\text{O})]_n \cdot n\text{H}_2\text{O}$ (**2**). Compound **2** was synthesized by adapting a procedure for **1** and using a mixture of H_2cpna (0.3 mmol, 77.7 mg) with phen (0.30 mmol 60.0 mg). Orange crystals (blocks) were removed from the reaction mixture manually or by filtration, washed with H_2O , and then air-dried to furnish **2**. Yield: 60%, based on H_2cpna . Analysis calculated for $\text{C}_{25}\text{H}_{19}\text{CoN}_3\text{O}_7$: C, 56.40; H, 3.60; N, 7.89. Found: C, 56.58; H, 3.62; N, 7.93%. IR (cm^{-1}): 3414w, 3062w, 1609s, 1564s, 1517w, 1492 w, 1453w, 1427w, 1395s, 1297w, 1244w, 1199w, 1160w, 1101w, 1043w, 1010w, 958w, 899w, 854m, 782m, 730w, 691w, 638w, 541w.

$[\text{Co}_3(\mu_4\text{-dppa})_2(\text{H}_2\text{O})_6]_n \cdot 2n\text{H}_2\text{O}$ (**3**). Compound **3** was synthesized by adapting a procedure for **1** and using H_3dppa (0.20 mmol, 57.4 mg) instead of H_2cpna . Pink crystals (blocks) were removed from the reaction mixture manually or by filtration, washed with H_2O , and then air-dried to furnish **3**. Yield: 60%, based on H_3dppa . Analysis calculated for $\text{C}_{28}\text{H}_{28}\text{Co}_3\text{N}_2\text{O}_{20}$: C, 37.82; H, 3.17; N, 3.15. Found: C, 37.95; H, 3.18; N, 3.12%. IR (cm^{-1}): 3387m, 1622s, 1596s, 1570w, 1486w, 1413s, 1368s, 1290w, 1251w, 1205w, 1160w, 1095w, 1036w, 899w, 841w, 808w, 782w, 704w, 658w, 638w, 541w.

$[\text{Co}_3(\mu_5\text{-dppa})_2(\mu\text{-4,4'-bipy})(\text{H}_2\text{O})_2]_n \cdot 4n\text{H}_2\text{O}$ (**4**). Compound **4** was synthesized by adapting a procedure for **1** and using a mixture of H_3dppa (0.20 mmol, 57.4 mg) with 4,4'-bipy (0.3 mmol, 46.8 mg)

Table 1. Crystallographic Data for Compounds **1–4**

	1	2	3	4
chemical formula	$\text{C}_{13}\text{H}_{11}\text{CoNO}_7$	$\text{C}_{25}\text{H}_{19}\text{CoN}_3\text{O}_7$	$\text{C}_{28}\text{H}_{28}\text{Co}_3\text{N}_2\text{O}_{20}$	$\text{C}_{38}\text{H}_{32}\text{Co}_3\text{N}_4\text{O}_{18}$
formula weight	352.16	532.36	889.31	1009.46
crystal system	monoclinic	monoclinic	triclinic	monoclinic
space group	$P2_1/n$	$P2_1/n$	$P\bar{1}$	$I2/c$
<i>a</i> , Å	6.1155(2)	12.1205(4)	7.4924(5)	25.592(2)
<i>b</i> , Å	8.1678(3)	10.2942(4)	9.5818(5)	7.2957(3)
<i>c</i> , Å	26.0705(10)	18.4120(6)	12.0040(9)	23.7096(18)
α , deg	90	90	88.207(5)	90
β , deg	92.335(4)	91.373(3)	75.573(6)	120.372(11)
γ , deg	90	90	76.919(5)	90
<i>V</i> , Å ³	1301.14(8)	2296.61(13)	812.66(10)	3819.3(6)
<i>T</i> , K	293(2)	293(2)	293(2)	293(2)
<i>Z</i>	4	4	1	4
<i>D_c</i> , g cm ⁻³	1.798	1.540	1.756	1.756
μ , mm ⁻¹	1.357	0.800	1.607	1.377
<i>F</i> (000)	716	1092	451	2052
reflms measured	4587	8123	5117	6800
unique reflms (<i>R_{int}</i>)	2306 (0.0355)	4071 (0.0388)	2853 (0.0203)	3396 (0.0450)
GOF on <i>F</i> ²	0.998	1.040	1.018	1.051
<i>R</i> ₁ [<i>I</i> > 2σ(<i>I</i>)]	0.0373	0.0442	0.0362	0.0466
<i>wR</i> ₂ [<i>I</i> > 2σ(<i>I</i>)]	0.0689	0.0827	0.0932	0.0921

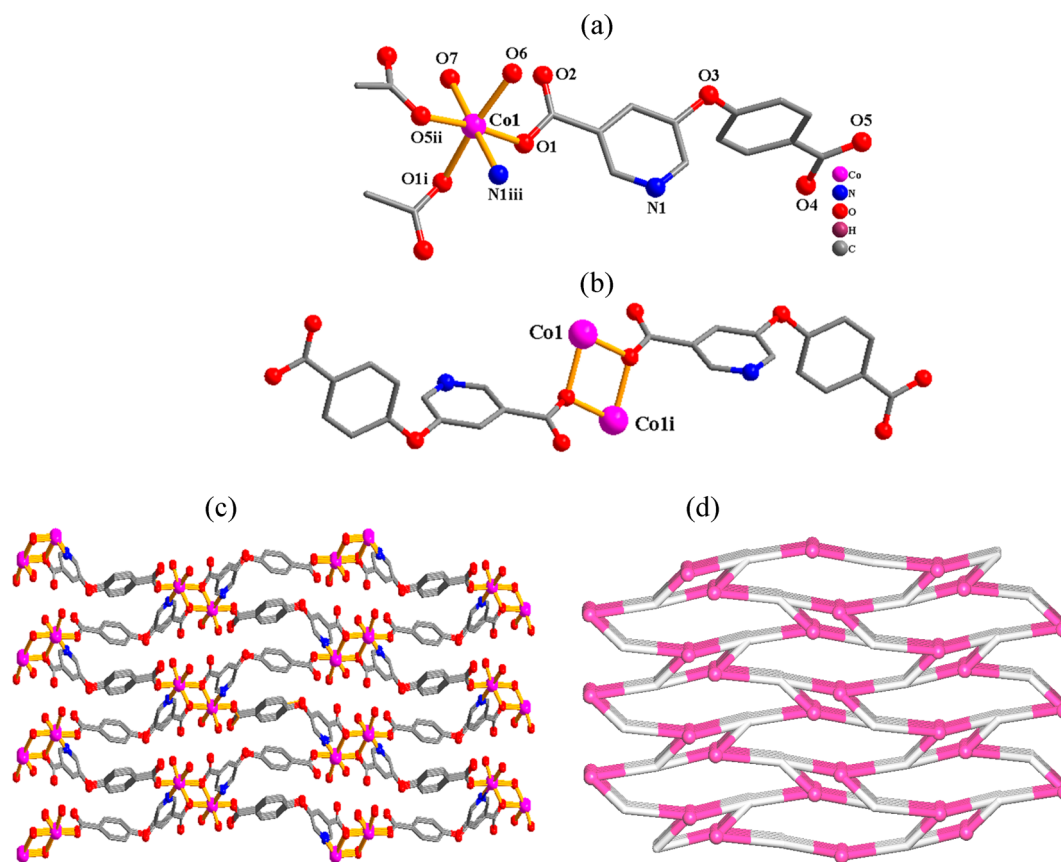


Figure 1. Crystal structure of MOF 1. (a) Co1 coordination environment. (b) Dicotbalt(II) carboxylate motif. (c) 3D metal–organic framework. (d) Simplified topological representation of 3D MOF displaying a 4-connected uninodal network of the *sra* topological type; centroids of 4-connected μ_4 -cpna²⁻ nodes (gray), 4-connected Co1 nodes (magenta balls). Further details: (a–c) H atoms are not shown; (c) view along the *b* plane; (d) view along the *a* axis.

instead of H₂cpna. Pink crystals (blocks) were removed from the reaction mixture manually or by filtration, washed with H₂O, and then air-dried to furnish 4. Yield: 62%, based on H₃dppa. Analysis calculated for C₃₈H₃₂Co₃N₄O₁₈: C, 45.21; H, 3.20; N, 5.55. Found: C, 45.07; H, 3.18; N, 5.52%. IR (cm⁻¹): 3590 w, 3498 w, 1596 s, 1564 s, 1492 w, 1401 s, 1257 w, 1212 w, 1160 w, 1095 w, 1062 w, 1036 w, 1010 w, 919 w, 847 w, 808 w, 704 m, 658 w, 625 w, 560 w.

Single-Crystal X-ray Diffraction. Single-crystal X-ray data of 1–4 were collected on a Bruker Smart CCD diffractometer ($\lambda = 0.71073$ Å, graphite-monochromated Mo $K\alpha$ radiation). The SADABS program was applied for semiempirical absorption corrections. Structures were solved by direct methods and refined by full-matrix least-squares on F^2 using SHELXS-97/SHELXL-97 programs.⁴⁰ All non-hydrogen atoms were anisotropically refined (full-matrix least-squares on F^2). CH hydrogen atoms were positioned in calculated sites with fixed isotropic thermal parameters; these were included in structure factor calculations when performing a final stage refinement. Water H atoms were located by difference maps and constrained to ride on the respective O atoms. Crystallographic data for compounds 1–4 are listed in Table 1, whereas Tables S1 and S2 (Supporting Information, SI) provide a summary of selected structural parameters.

Catalytic Study. Alcohol oxidation reactions were investigated under vigorous stirring in an air atmosphere in glass reactors (thermostated at 50 °C) that were equipped with a reflux condenser. In a typical test, a heterogeneous Co(II) catalyst selected from 1–4 (5 μ mol; calculated per one cobalt atom) and CH₃CN solvent (up to 5 mL) were added to a glass reactor and then alcohol (1 mmol), nitromethane (GC internal standard, 0.2 M final concentration), and oxidant (*t*BuOOH, 70% in H₂O, 7 mmol) were introduced. Progress of catalytic reactions was observed by periodically taking samples from reaction mixture. Prior to GC analysis, these samples were mixed with

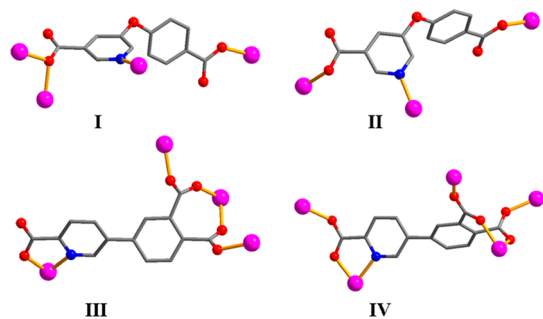
a small amount of solid triphenylphosphine (Shul’pin’s method^{41,42}) to reduce the remaining peroxide. GC peaks were attributed based on chromatograms of commercial samples. Blank tests indicated that oxidation reactions are significantly slower in the absence of Co catalyst (Figure S7). A slightly elevated temperature of 50 °C is essential for the activation of *t*BuOOH oxidant; in fact, the reaction rates at 50 and 20 °C differ by more than 20-fold (for catalyst 2, Figure S7). Acetonitrile was selected as a standard solvent for this type of reactions due to its stability toward oxidation, sufficient boiling point, and solvation properties.³¹

RESULTS AND DISCUSSION

Structural Description. $[Co(\mu_4\text{-cpna})(H_2O)_2]_n$ (1). Cobalt(II) product 1 is a three-dimensional MOF (Figure 1) that is composed of a Co(II) center, a μ_4 -cpna²⁻ block, and two H₂O molecules of crystallization (per asymmetric unit). The six-coordinate Co1 atom displays a slightly distorted {CoNO₅} octahedral environment (Figure 1a), which is occupied by three oxygen and one nitrogen donor atoms coming from four different μ_4 -cpna²⁻ moieties, in addition to a couple of terminal H₂O ligands. The Co–N [2.157(3) Å] and Co–O [2.053(2)–2.199(2) Å] distances are typical for the present type of Co(II) compounds.^{7a,18,27} The cpna²⁻ block behaves as a μ_4 -N,O₂-ligand, wherein the COO⁻ groups are monodentate or bidentate (Scheme 2, mode I); the dihedral angle between pyridyl and benzene functionalities attains 85.13°, while the C–O_{ether}–C angle is 118.17°.

Two μ -carboxylate O atoms of two μ_4 -cpna²⁻ spacers interlink the adjacent Co(II) centers into the dicobalt(II)

Scheme 2. Modes of Coordination of Main Ligands ($\mu_3\text{-cpna}^{2-}$: Modes I and II; dppa^{3-} : Modes III and IV) in Compounds 1–4



motifs (Figure 1b) with a $\text{Co}\cdots\text{Co}$ separation of 3.350(2) Å. Such motifs are further assembled, via the remaining COO^- groups and N atoms of $\mu_4\text{-cpna}^{2-}$, to a three-dimensional MOF (Figures 1c, S1, and S2). After simplification, topological classification of this 3D MOF (Figure 1d) reveals a 4-connected uninodal net of *sra* topological type; the point symbol is $(4^2.6^3.8)$.

$[\text{Co}(\mu_3\text{-cpna})(\text{phen})(\text{H}_2\text{O})]_n \cdot n\text{H}_2\text{O}$ (**2**). Compound **2** features a two-dimensional coordination polymer network (Figure 2). The asymmetric unit is composed of a Co(II) center, a $\mu_3\text{-cpna}^{2-}$ block, a phen moiety, a terminal water ligand, and a lattice H_2O molecule (Figure 2a). The six-coordinate Co1 center shows a distorted $\{\text{CoN}_3\text{O}_3\}$ octahedral geometry. It is occupied by two oxygen and one nitrogen atoms from three $\mu_3\text{-cpna}^{2-}$ spacers, a pair of phen N atoms, and an H_2O ligand, with the standard Co-N [2.138(3)–2.170(3) Å] and Co-O [2.030(2)–2.145(3) Å] distances.^{7b,27,28} In **2**, cpna^{2-} behaves as the $\mu_3\text{-N,O}_2$ -ligand (mode II, Scheme 2) in which both carboxylate groups are monodentate; a $\text{C-O}_{\text{ether}}\text{-C}$ angle is 115.77° , while a dihedral angle between the rings of cpna^{2-} is

76.35° . The $\mu_3\text{-cpna}^{2-}$ spacers interlink the Co1 centers into a two-dimensional layer (Figures 2b and S3), wherein both the Co1 and $\mu_3\text{-cpna}^{2-}$ nodes are 3-connected and equivalent from a topological point of view (Figure 2c). A simplified layer (Figure 2c) is topologically described as the 3-connected uninodal net with the *fes* topology and the point symbol of (4.8^2) .

$[\text{Co}_3(\mu_4\text{-dppa})_2(\text{H}_2\text{O})_6]_n \cdot 2n\text{H}_2\text{O}$ (**3**). Product **3** also displays a two-dimensional coordination polymer structure (Figure 3). However, **3** is more complex than **2** given the presence of two different Co(II) centers (Co2 with a full occupancy; Co1 with a half occupancy), one $\mu_4\text{-dppa}^{3-}$ spacer, three water ligands, and a lattice H_2O molecule per asymmetric unit (Figure 3a). Co1 atom is six-coordinate and is located on a 2-fold rotation axis. It adopts an ideal octahedral $\{\text{CoO}_6\}$ geometry, which is taken by four oxygen donors (from four $\mu_4\text{-dppa}^{3-}$ spacers) and two terminal water ligands. The Co2 atom also features a slightly distorted $\{\text{CoNO}_5\}$ octahedral environment that is filled by three carboxylate oxygen and one nitrogen atoms from two $\mu_4\text{-dppa}^{3-}$ spacers, in addition to two terminal water ligands. The Co-N distance is 2.122(3) Å, whereas the Co-O bonds range from 2.032(2) to 2.142(2) Å; these distances are in accord with related cobalt derivatives.^{18,27,29} The dppa^{3-} block functions as the μ_4 -ligand (Scheme 2, mode III), in which carboxylate groups are bridging bidentate or monodentate. In $\mu_4\text{-dppa}^{3-}$, a dihedral angle among the picolinate and isophthalate functionalities attains 31.29° . Both Co1/Co2 centers are interlinked by neighboring carboxylate groups (phthalate functionality of $\mu_4\text{-dppa}^{3-}$) to generate a one-dimensional double chain pattern (Figure 3b). These patterns are extended further, through a picolinate functionality of $\mu_4\text{-dppa}^{3-}$, into a complex 2D layer (Figure 3c). From a topological perspective, a simplified 2D net of this CP is built from the 3-connected $\mu_4\text{-dppa}^{3-}$ nodes, the 4-connected Co1 nodes, and the 2-connected Co2 atoms acting as linkers (Figure 3d). Topological classification reveals a 3,4-connected

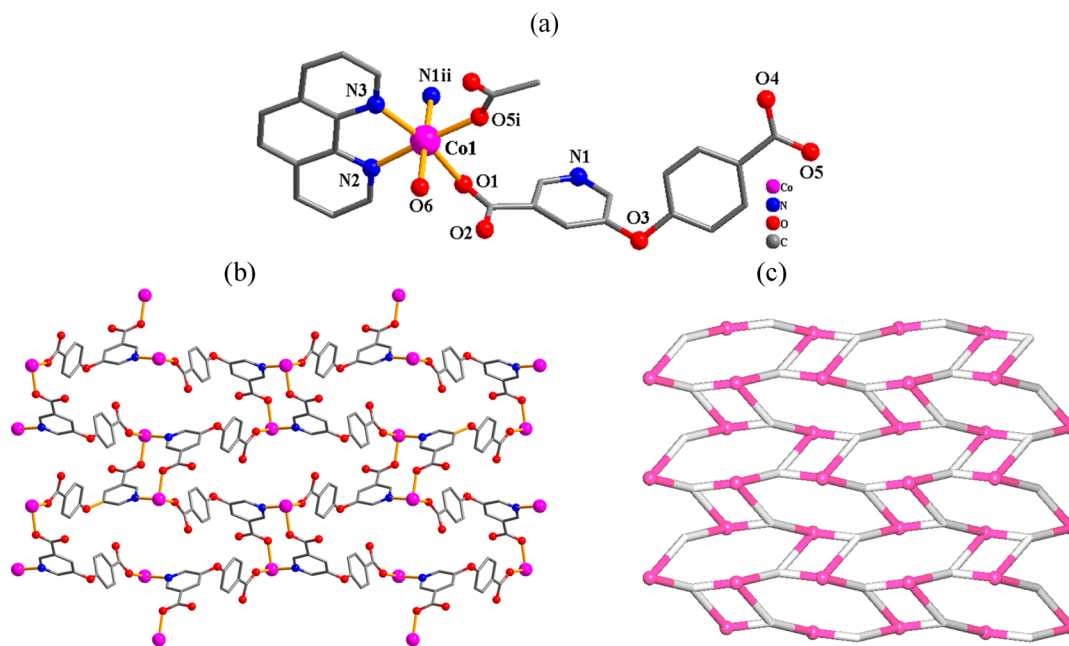


Figure 2. Crystal structure of **2**. (a) Co1 coordination environment. (b) 2D metal–organic layer. (c) Simplified topological representation of 2D layer displaying a 3-connected uninodal net of the *fes* topological type; 3-connected Co1 nodes (magenta balls), centroids of 3-connected $\mu_3\text{-cpna}^{2-}$ nodes (gray). Further details: (a, b) H atoms and phen ligands in (b) are not shown; (b) view along the *bc* plane; (c) view along the *a* axis.

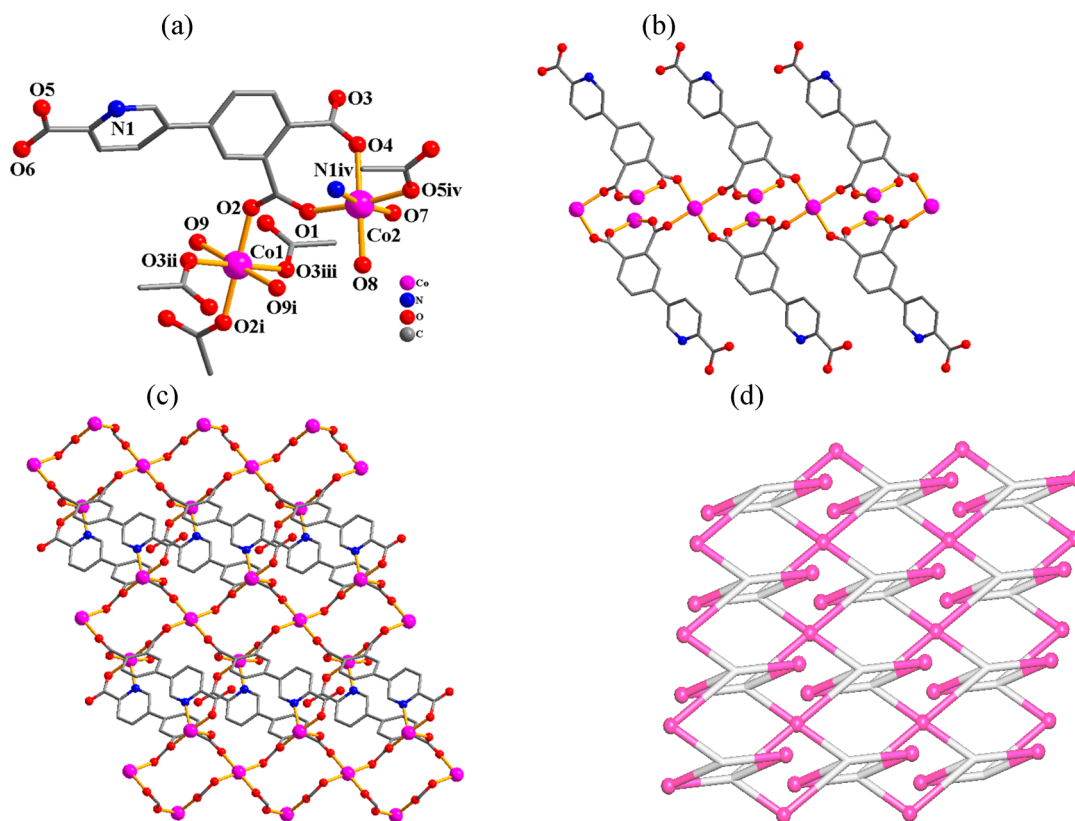


Figure 3. Crystal structure of **3**. (a) Co1 and Co2 coordination environment. (b) 1D double chain motif. (c) 2D metal–organic layer. (d) Simplified topological view of two-dimensional CP showing a 3,4-connected binodal layer of the 3,4L13 topological type; centroids of 3-connected μ_4 -dppa $^{3-}$ nodes (gray), 2-connected Co2 linkers, and 4-connected Co1 nodes (magenta balls). Further details: (a–c) H atoms are not shown; (b) view along the *bc* plane; (c, d) view along the *b* axis.

binodal net of the 3,4L13 topological type. This net is defined by the $(4.6^2)_2(4^2.6^2.8^2)$ point symbol in which the (4.6^2) and $(4^2.6^2.8^2)$ notations refer to the μ_4 -dppa $^{3-}$ and Co1 nodes, correspondingly.

$[\text{Co}_3(\mu_5\text{-dppa})_2(\mu\text{-}4,4'\text{-bipy})(\text{H}_2\text{O})_2]_n \cdot 4n\text{H}_2\text{O}$ (**4**). If compared to **3**, the structure of **4** possesses a more intricate 3D metal–organic framework due to the presence of an additional $\mu\text{-}4,4'$ -bipy linker (Figure 4). The asymmetric unit of **4** bears two Co(II) atoms (Co1 with a complete and Co2 with a half occupancy), a μ_5 -dppa $^{3-}$ block, a half of $\mu\text{-}4,4'$ -bipy moiety, a H₂O ligand, and two lattice H₂O molecules. The Co2/Co1 atoms are six-coordinate and possess the octahedral $\{\text{CoO}_6\}$ and $\{\text{CoN}_2\text{O}_4\}$ environments, correspondingly (Figure 4a). The Co1 atom is bound by four oxygen and one nitrogen donors coming from three μ_5 -dppa $^{3-}$ ligands, in addition to one $4,4'$ -bipy N donor. The Co2 atom is surrounded by four oxygen donors of μ_5 -dppa $^{3-}$ blocks and a couple of terminal H₂O ligands. The Co–N and Co–O bonds are in the 2.156(4)–2.176(4) and 2.066(3)–2.139(3) Å range, respectively. The dppa $^{3-}$ block acts as a μ_5 -N,O₆-spacer with all three COO[−] groups adopting a bidentate bridging fashion (mode IV, Scheme 2). The μ_5 -dppa $^{3-}$ block features the dihedral angle of 48.19° (angle involving the aromatic rings). Carboxylate groups of μ_5 -dppa $^{3-}$ provide an interconnection of cobalt(II) centers into a 2D sheet pattern (Figure 4b). Such patterns are extended further, via an additional functionality of μ_5 -dppa $^{3-}$ and the $\mu\text{-}4,4'$ -bipy linkers, into a 3D MOF structure (Figure 4c).

Topologically, a simplified net of **4** is built from the Co1 and Co2 nodes (both are 4-connected but topologically distinct),

5-connected μ_5 -dppa $^{3-}$ nodes, and 2-connected $\mu\text{-}4,4'$ -bipy linkers (Figure 4d). Hence, MOF **4** discloses a 4,4,5-connected trinodal underlying net of a unique topological type. This is defined by the $(4.5^2.6.7.8)_2(4^2.5^2.6^2.7^3.8)_2(4^2.5^2.6^2)$ point symbol, wherein the $(4.5^2.6.7.8)$, $(4^2.5^2.6^2.7^3.8)$, and $(4^2.5^2.6^2)$ indices belong to Co1, μ_5 -dppa $^{3-}$, and Co2 nodes, correspondingly. The unique type of this topology can be attested by screening of various databases.^{43–46} Further simplification of this framework ($\mu\text{-}4,4'$ -bipy linkers omitted) results in a trinodal net with a rare **pkb2** topology.⁴³

Synthesis and Structural Comparison of 1–4. Compounds **1** and **2** were obtained by performing similar syntheses but using phen as an additional mediator of crystallization when preparing product **2**. In this case, phen chelator can block two coordination sites of cobalt(II) ions, resulting in a structure of lower dimensionality (2D CP **2** vs 3D MOF **1**). In contrast, the use of $4,4'$ -bipy as an additional linker and crystallization mediator when synthesizing **4** gives rise to a more complex structure (3D MOF **4** vs 2D CP **3**). These results show that the use of an *N,N*-type crystallization mediator affects the final structure and dimensionality of the metal–organic network during the hydrothermal synthesis. Compounds **1–4** are nonporous as attested by the calculation of an effective free volume of the crystal volume by PLATON, showing that the unit cell contains no residual solvent accessible voids.

In compounds **1–4**, the cpna $^{2-}$ and dppa $^{3-}$ blocks are fully deprotonated and show diverse coordination modes (Scheme 2), ranging from μ_4 -N,O₂-cpna $^{2-}$ and μ_3 -N₂O₂-cpna $^{2-}$ (in **1** and **2**) to μ_4 -N,O₅-dppa $^{3-}$ and μ_5 -N,O₆-dppa $^{3-}$ (in **3** and **4**). To

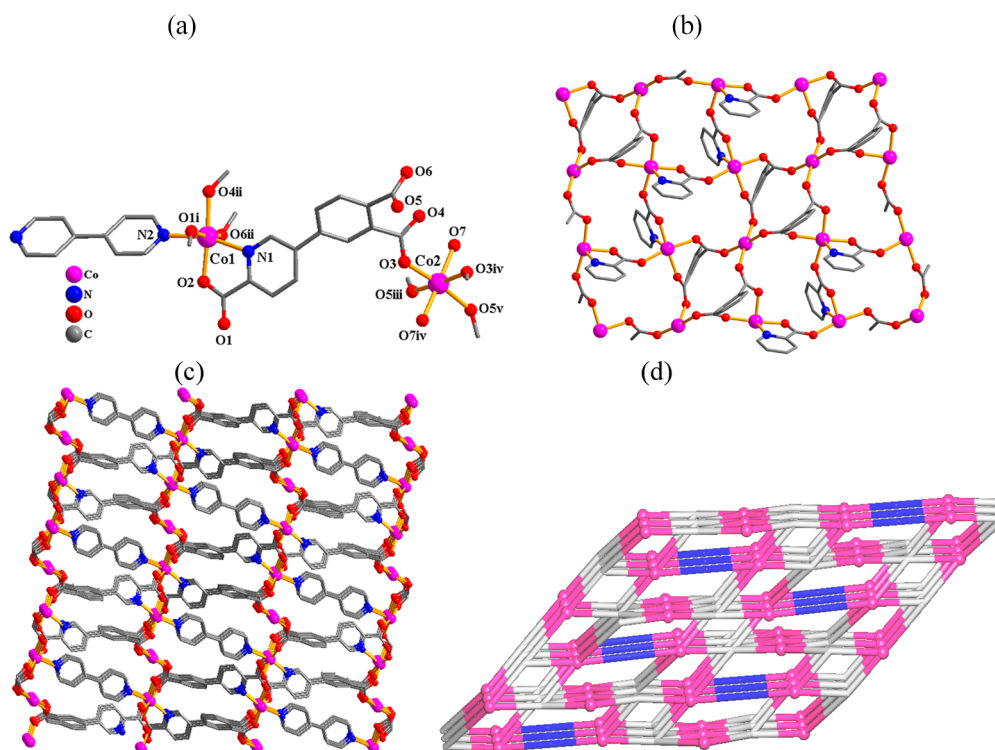


Figure 4. Crystal structure of 4. (a) Co1 and Co2 coordination environment. (b) 2D layer pattern. (c) 3D MOF. (d) Simplified representation of 3D MOF displaying a 4,4,5-connected trinodal underlying framework of the new topological type; centroids of 5-connected μ_5 -dppa³⁻ nodes (gray), 4-connected Co1/Co2 nodes (magenta balls), centroids of 2-connected μ -4,4'-bipy linkers (blue). Further details: (a–c) H atoms are not shown; (b) view along the *ab* plane; (c) view along the *ac* plane; (d) view along the *b* axis.

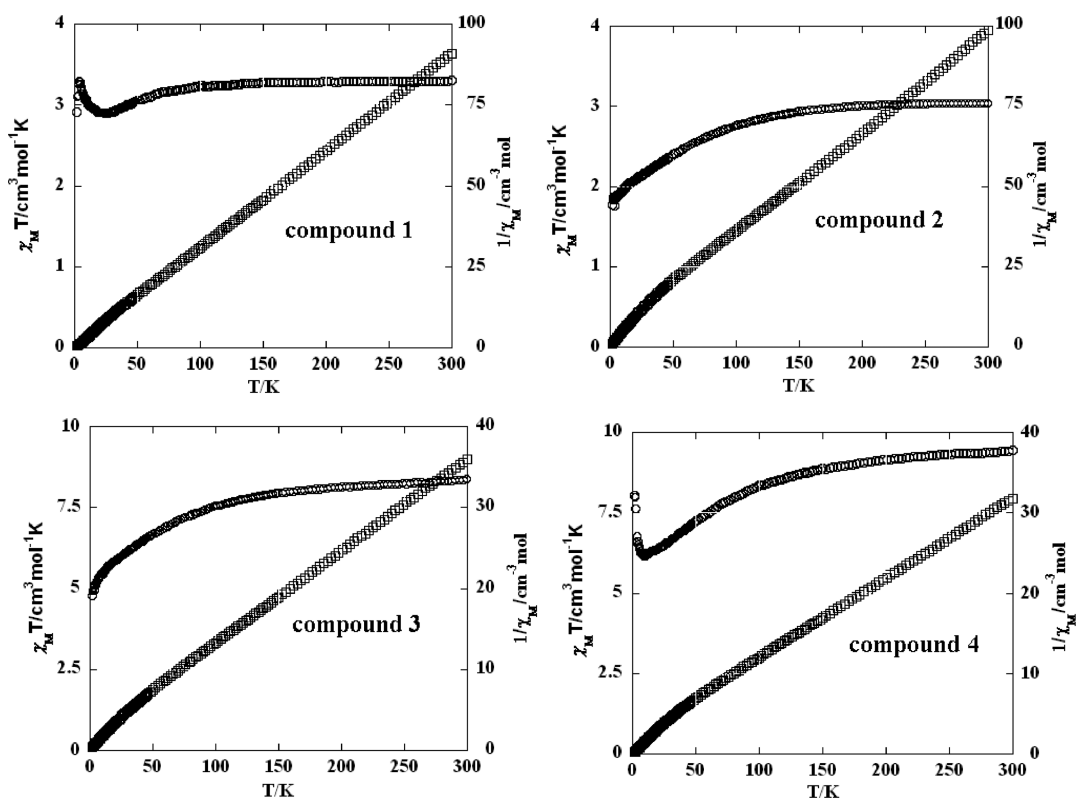


Figure 5. Magnetic susceptibility data for compounds 1–4 ($\chi_M T$ (○) and $1/\chi_M$ (□) vs *T*).

achieve a required coordination geometry at cobalt(II) centers, both pyridine-carboxylate ligands undergo some rotation of aromatic rings owing to the presence of the C–O_{ether}–C and

C–C functionality, with respective angles of 115.77–118.17° (C–O_{ether}–C angle in cpna²⁻) and 31.29–48.19° (dihedral angle in dppa³⁻).

Apart from distinct dimensionalities, the obtained compounds also feature different types of topological networks, namely, (a) 4-connected uninodal 3D framework of an *sra* (SrAl_2) topological type in compound **1**, (b) 3-connected uninodal layer with an *fes* [Shubnikov plane net (4.8^2)] topology in compound **2**, (c) 3,4-connected binodal layer of a $3,4L13$ topological type in compound **3**, and (d) 4,4,5-connected trinodal framework of the novel topological type in compound **4**.

TGA and PXRD Results. Thermogravimetric analysis (TGA) was used to investigate the stability of compounds **1–4** upon heating under a flow of N_2 (Figure S4, SI). A loss of two H_2O ligands in **1** (calcd, 10.2%; exptl, 10.4%) is observed at a rather high temperature interval (151–297 °C); the dehydrated sample then decomposes starting at 351 °C. TGA data of **2** show two minor thermal effects in the 61–195 °C range, which are associated with a release of one solvent H_2O molecule and one water ligand (calcd, 6.8%; exptl, 6.5%). After dehydration, the sample of **2** is stable until 297 °C. For compound **3**, two thermal effects in the 92–230 °C temperature range refer to the loss of two crystallization water molecules and six H_2O ligands (calcd, 16.2%; exptl, 16.3%); the sample then starts to decompose at 331 °C. Two minor thermal effects are also observed in the 116–258 °C interval in the TGA plot of **4**, which correspond to the removal of four solvent molecules and a couple of H_2O ligands (calcd, 10.7%; exptl, 10.3%). After dehydration, the sample maintains stability up to 380 °C.

Powder X-ray diffraction (PXRD) experiments were undertaken using microcrystalline samples of **1–4**. The obtained powder diffractograms (Figure S5, SI) well match the calculated patterns (on the basis of single-crystal X-ray diffraction data). This proves a phase homogeneity of the as-synthesized compounds.

Magnetic Properties. Magnetic susceptibility study at different temperatures (2–300 K) was performed using the crystalline samples of cobalt(II) compounds **1–4** (Figure 5). For **1**, the $\chi_{\text{M}}T$ value of $3.30 \text{ cm}^3 \cdot \text{mol}^{-1} \cdot \text{K}$ at 300 K is superior if compared to the value ($1.83 \text{ cm}^3 \cdot \text{mol}^{-1} \cdot \text{K}$) calculated for one isolated (magnetically) high-spin cobalt(II) ion ($g = 2.0$, $S = 3/2$). Such an observation represents a phenomenon commonly seen for cobalt(II) ions owing to powerful spin–orbital coupling.^{18,27,29} The $\chi_{\text{M}}T$ values slowly decline to $2.89 \text{ cm}^3 \cdot \text{mol}^{-1} \cdot \text{K}$ (minimum value) on decreasing the temperature up to 24 K. Further decrease of the temperature to 4 K leads to an abrupt increase of $\chi_{\text{M}}T$ ($3.29 \text{ cm}^3 \cdot \text{mol}^{-1} \cdot \text{K}$), which then quickly decreases on further cooling.

For **2**, the $\chi_{\text{M}}T$ value at 300 K ($3.04 \text{ cm}^3 \cdot \text{mol}^{-1} \cdot \text{K}$) is higher than the parameter ($\chi_{\text{M}}T = 1.83 \text{ cm}^3 \cdot \text{mol}^{-1} \cdot \text{K}$) expected for an isolated high-spin cobalt(II) ion ($g = 2.0$, $S = 3/2$). Upon cooling from 300 to 2 K, $\chi_{\text{M}}T$ decreases from 3.04 to $1.77 \text{ cm}^3 \cdot \text{mol}^{-1} \cdot \text{K}$, respectively (Figure 5). Such a decrease of $\chi_{\text{M}}T$ can be explained by the general antiferromagnetic interaction between cobalt(II) centers.

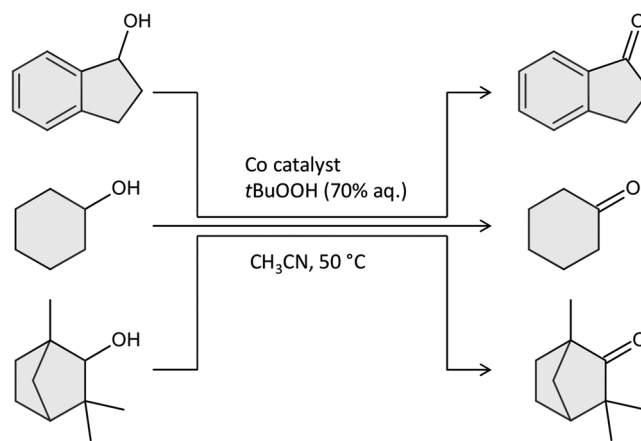
For compound **3**, room temperature $\chi_{\text{M}}T$ ($8.36 \text{ cm}^3 \cdot \text{mol}^{-1} \cdot \text{K}$) is significantly higher than the value of $5.61 \text{ cm}^3 \cdot \text{mol}^{-1} \cdot \text{K}$ expected for three isolated Co(II) ions ($S = 3/2$), indicating the presence of a significant spin–orbital coupling. On decreasing the temperature, $\chi_{\text{M}}T$ values steadily go down, suggesting the dominant antiferromagnetic interactions within the spin network.

Metal–organic framework **4** shows a room temperature $\chi_{\text{M}}T$ of $9.44 \text{ cm}^3 \cdot \text{mol}^{-1} \cdot \text{K}$, which is significantly higher if compared

to a value ($5.61 \text{ cm}^3 \cdot \text{mol}^{-1} \cdot \text{K}$) expected for three isolated high-spin Co(II) ions ($S = 3/2$). This can be explained by the significant orbital contribution.^{7a,27,29} The value of $\chi_{\text{M}}T$ declines to $6.13 \text{ cm}^3 \cdot \text{mol}^{-1} \cdot \text{K}$ (minimum value) on decreasing the temperature to 10 K, followed by an abrupt increase to $8.03 \text{ cm}^3 \cdot \text{mol}^{-1} \cdot \text{K}$ (maximum value) at 2 K, thus showing a complex behavior. According to the structure of **4** (Figure 4b), adjacent Co(II) centers possess a single type of the magnetic exchange path, namely, through one *syn-anti* carboxylate bridge, which explains a ferromagnetic exchange observed in this compound.

Catalytic Study. Catalytic performance of **1–4** was evaluated for oxidation of alcohols with peroxides under mild conditions (Scheme 3). The compounds **1–4** were hydro-

Scheme 3. Mild Oxidation of Alcohols to Ketones Catalyzed by **1–4**



thermally generated and are stable in water (Figure S5, SI). They are insoluble in the catalytic reaction medium composed of an alcohol substrate, aqueous *t*BuOOH oxidant, and acetonitrile solvent, thus acting as heterogeneous catalysts.

Oxidation of 1-indanol (0.2 M) with *tert*-butylhydroperoxide (*t*BuOOH; 1.4 M) catalyzed by **1–4** (0.5 mol %) in acetonitrile afforded 1-indanone as a main reaction product. The highest product yield (45%) was observed for the catalyst **2**, followed by **1**, **4**, and **3** (26–39% yields, Table 2).

Table 2. Mild Oxidation of Alcohols with *t*BuOOH Catalyzed by **1–4**^a

substrate/catalyst	yield of ketone (%) ^b			
	1	2	3	4
1-indanol	39.4	44.5	26.3	37.0
cyclohexanol	9.6	20.9	9.0	7.1
fenchyl alcohol	6.1	7.3	5.0	5.6

^aReaction conditions: Co catalyst (5 μmol ; 0.5 mol %), alcohol (1 mmol), *t*BuOOH (aq. 70%, 7 mmol), acetonitrile (until 5 mL of total reaction volume), 24 h, 50 °C. ^bMolar yield based on substrate: (moles of ketone product per mol of alcohol substrate) \times 100%.

The accumulation plots of 1-indanone (Figure 6) exhibit a linear dependence for all the catalysts, with almost equal initial reaction rates for **1**, **3**, and **4** of $8.4 \times 10^{-7} \text{ M s}^{-1}$ and a considerably higher rate of $1.5 \times 10^{-6} \text{ M s}^{-1}$ for compound **2** (Figure 6).

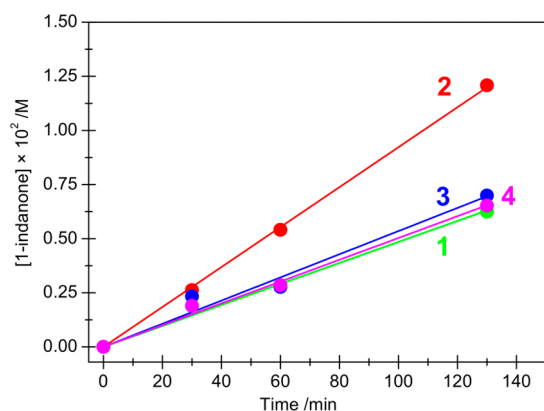


Figure 6. Accumulation of 1-indanone vs time in the 1-indanol oxidation by *t*BuOOH in the presence of catalysts 1–4 (conditions of the reactions are those of Table 2).

Cyclohexanol can also be used as a substrate, leading to a maximum cyclohexanone yield of 21% for **2** and 7–10% for **1**, **3**, and **4** (Table 2). Similarly to 1-indanol, compound **2** exhibits the highest activity among all the catalysts studied. In contrast to 1-indanone (Figure 6), the accumulation curves for cyclohexanone demonstrate a complex behavior with a quasi-linear dependence in the 30–150 min range (Figure S6, SI). Replacement of cyclohexanol by a structurally related fenchyl alcohol (Figure S6, SI) caused only a slight change in the product yield when using **1**, **3**, and **4** after 24 h (Table 2), while a yield drop was observed in the system catalyzed by **2**. Notably, all the catalytic systems exhibit almost 100% selectivity in the case of cyclohexanol and fenchyl alcohol oxidation, as no byproducts were detected. In the case of 1-indanol oxidation, the selectivity to 1-indanone is at the 85% level.

The highest yield of 1-indanone as comparing to other substrates can be explained by an enhanced activity of the proton located at the benzylic position; activation of this proton is a required step. The same reason can explain a lower selectivity in the oxidation of 1-indanol, where activation of the second benzylic C–H bond can produce various products up to 1,3-indandione. Lower activity of the fenchyl alcohol relative to cyclohexanol can be due to a pronounced sterical hindering of the methyl and methylene groups close the alcohol one.

Although all the compounds **1**–**4** are insoluble in the reaction medium and act as heterogeneous catalysts; some leaching of cobalt(II) ions can be detected at a prolonged reaction time, as confirmed by chelation experiments with 2,2'-bipyridine (bpy).^{33a} In contrast to a linear dependence of the ketone accumulation demonstrated by **2** (Figure S7), the 2+bpy system shows acceleration with the initial reaction rate W_0 of $2.3 \times 10^{-6} \text{ M s}^{-1}$. Such a reaction rate is very close to that observed (Figure S7) for the system containing only **2** ($1.5 \times 10^{-6} \text{ M s}^{-1}$). This behavior can be explained by a small leaching of the cobalt ions during the reaction. At a low concentration, homogeneous cobalt species do not show notable activity and the accumulation curves for **1**–**4** remain linear. On the other side, introduction of bpy as a strong chelator may additionally contribute to a disaggregation of the heterogeneous catalyst, leading to generation of homogeneous Co-bpy species.

Although yields of products exhibited by the catalysts **1**–**4** are moderate if compared to other heterogeneous catalysts,^{47,48} it should be noted that, in the case of **1**–**4**, the lower yields are

due to a low catalyst loading of 0.5 mol %, as a main scope of the present study was to investigate kinetic effects of the catalysts rather than to optimize the reaction to achieve high yields. In comparison, a series of Co(II)-cluster-based MOFs in a very high loading (20 mol %) can produce up to 90% of 1-indanone yield in the oxidation of indane with *t*BuOOH.⁴⁹ Despite showing modest activity, different cobalt salts can also be applied as simple homogeneous catalysts for the oxidation of alcohols with *t*BuOOH.^{49,50}

We also investigated an influence of the oxidant type on product yields using a catalytic system that revealed the highest activity. In fact, the oxidation of 1-indanol with H_2O_2 , catalyzed by **2**, showed a low yield of 1-indanone (4%) after 24 h. A slightly higher yield (7%) but with a very low selectivity of 6% was observed when using peracetic acid ($\text{CH}_3\text{CO}_3\text{H}$) as a terminal oxidant (conversion of 1-indanol was 97% with formation of a wide range of oxidation products). The use of 3-chloroperbenzoic acid improved the yield of 1-indanone up to 47%, which is comparable with the system operating with the *t*BuOOH oxidant. Finally, we attempted to perform the aerobic oxidation, as some coordination compounds of cobalt are known to catalyze the oxidation of alcohols with dioxygen.²⁵ However, no 1-indanone or any other product was detected. These data suggest that *t*BuOOH is a preferable oxidant in the present Co-catalyzed oxidation of alcohols. Better reactivity of *t*BuOOH in comparison with H_2O_2 can be related to an enhanced miscibility of the former with organic solvents. Besides, *t*BuOOH is more stable and not prone to O_2 release at high concentrations (this side reaction is very typical for H_2O_2). Despite showing high reactivity, peracids as oxidants typically lead to overoxidation products due to Baeyer–Villiger oxidation of ketones and other processes, thus resulting in a low overall selectivity.

CONCLUSIONS

We showed that new types of cobalt(II) CPs and MOFs can be easily generated, by hydrothermal synthesis in water, from Co(II) chloride and two flexible and still very poorly explored pyridine-carboxylic acid ligands (H_2cpna and H_3dppa). The structures of the obtained products vary from 2D metal-organic layers (**2** and **3**) to 3D frameworks (**1** and **4**) and feature different topologies and architectures, which also include unique types. An observed diversity of the structures of **1**–**4** suggests that both a main pyridine-carboxylate ligand and an optional *N,N*-donor crystallization mediator affect the construction and resulting structures of these CPs or MOFs.

Thermal and aqueous stability, and catalytic and magnetic properties of compounds **1**–**4** were studied as well. In particular, catalytic studies disclosed that **1**–**4** are active heterogeneous catalysts in the oxidation of alcohols with *t*BuOOH. Compound **2**, bearing $\mu_3\text{-cpna}^{2-}$ and phen ligands, revealed a considerably higher activity than the other products, suggesting a particular catalytic efficiency of such a combination of ligands.

Furthermore, the obtained products **1** and **2** represent a rare type of coordination polymers assembled from H_2cpna , while compounds **3** and **4** are the first Co(II) CPs assembled from H_3dppa , according to the Cambridge Structural Database (CSD). Hence, the present study also widened an application of such flexible pyridine-carboxylate blocks toward designing new metal-organic architectures. Further research with a focus on assembling related cobalt(II) CPs and MOFs and on the

exploration of their functional properties is in progress. In particular, the development of more stable, efficient, and recoverable heterogeneous catalytic systems for the oxidation of alcohols and other organic substrates will be pursued.

■ ASSOCIATED CONTENT

📄 Supporting Information

The Supporting Information is available free of charge on the ACS Publications website at DOI: 10.1021/acs.inorgchem.9b00242.

Selected bond lengths (Table S1) and H-bond parameters (Table S2), additional figures with representation of crystal structures (Figures S1–S3), TGA (Figure S4) and PXRD data (Figure S5), kinetic curves (Figures S6 and S7) (PDF)

Accession Codes

CCDC 1874595–1874598 contain the supplementary crystallographic data for this paper. These data can be obtained free of charge via www.ccdc.cam.ac.uk/data_request/cif, or by emailing data_request@ccdc.cam.ac.uk, or by contacting The Cambridge Crystallographic Data Centre, 12 Union Road, Cambridge CB2 1EZ, UK; fax: +44 1223 336033.

■ AUTHOR INFORMATION

Corresponding Authors

*E-mail: gujzh@lzu.edu.cn. Tel.: +86-931-8915196 (J.G.).

*E-mail: kirillov@tecnico.ulisboa.pt. Tel.: +351-218417178 (A.M.K.).

ORCID

Jinzhong Gu: 0000-0001-6704-7370

Zifa Shi: 0000-0001-9231-5963

Dmytro S. Nesterov: 0000-0002-1095-6888

Alexander M. Kirillov: 0000-0002-2052-5280

Notes

The authors declare no competing financial interest.

■ ACKNOWLEDGMENTS

The present work has been financially supported by the National Natural Science Foundation of China (Project 21201091), the Foundation for Science and Technology (FCT), and Portugal 2020 (projects IF/01395/2013/CP1163/CT005, CEECIND/03708/2017, UID/QUI/00100/2013, IST-ID/086/2018, and LISBOA-01-0145-FEDER-029697). The publication was also prepared with the support of the RUDN University Program 5-100. A.M.K. acknowledges the COST Action CA15106 (CHAOS).

■ REFERENCES

(1) (a) *The Chemistry of Metal-Organic Frameworks: Synthesis, Characterization, and Applications*; Kaskel, S., Ed.; Wiley-VCH: Weinheim, Germany, 2016; Vols. 1 and 2. (b) *Metal-Organic Framework Materials*; MacGillivray, L. R., Lukehart, C. M., Eds.; John Wiley & Sons: Chichester, U.K., 2014. (c) Batten, S. R.; Neville, S. M.; Turner, D. R. *Coordination Polymers: Design, Analysis and Application*; RSC: Cambridge, U.K., 2009. (d) Zhou, H.-C.; Long, J. R.; Yaghi, O. M. Introduction to metal–organic frameworks. *Chem. Rev.* **2012**, *112*, 673–674.

(2) (a) Kirchon, A.; Feng, L.; Drake, H. F.; Joseph, E. A.; Zhou, H. C. From fundamentals to applications: a toolbox for robust and multifunctional MOF materials. *Chem. Soc. Rev.* **2018**, *47*, 8611–8638. (b) Cui, Y. J.; Li, B.; He, H. J.; Zhou, W.; Chen, B. L.; Qian, G. D. Metal-organic frameworks as platforms for functional materials.

Acc. Chem. Res. **2016**, *49*, 483–493. (c) Yin, Z.; Wan, S.; Yang, J.; Kurmoo, M.; Zeng, M.-H. Recent advances in post-synthetic modification of metal-organic frameworks: New types and tandem reactions. *Coord. Chem. Rev.* **2019**, *378*, 500–512.

(3) (a) Zheng, X. D.; Lu, T. B. Constructions of helical coordination compounds. *CrystEngComm* **2010**, *12*, 324–336. (b) Lu, W. G.; Su, C. Y.; Lu, T. B.; Jiang, L.; Chen, J. M. Two stable 3D metal-organic frameworks constructed by nanoscale cages via sharing the single-layer walls. *J. Am. Chem. Soc.* **2006**, *128*, 34–35.

(4) (a) Yuan, S. A.; Zou, L. F.; Li, H. X.; Chen, Y. P.; Qin, J. S.; Zhang, Q.; Lu, W. G.; Hall, M. B.; Zhou, H. C. Flexible zirconium metal-organic frameworks as bioinspired switchable catalysts. *Angew. Chem., Int. Ed.* **2016**, *55*, 10776–10780. (b) Zhao, S. N.; Song, S. Z.; Song, S. Y.; Zhang, H. J. Highly efficient heterogeneous catalytic materials derived from metal-organic framework supports/precursors. *Coord. Chem. Rev.* **2017**, *337*, 80–96. (c) Xia, Q. C.; Li, Z. J.; Tan, C. X.; Liu, Y.; Gong, W.; Cui, Y. Multivariate metal-organic frameworks as multifunctional heterogeneous asymmetric catalysts for sequential reactions. *J. Am. Chem. Soc.* **2017**, *139*, 8259–8266. (d) Castro, K.; Figueira, F.; Mendes, R. F.; Cavaleiro, J. A. S.; Neves, M.; Simoes, M. M. Q.; Almeida Paz, F. A.; Tome, J. P.; Nakagaki, S. Copper-porphyrin-metal-organic frameworks as oxidative heterogeneous catalysts. *ChemCatChem* **2017**, *9*, 2939–2945.

(5) (a) Murray, L. J.; Dinca, M.; Long, J. R. Hydrogen storage in metal-organic frameworks. *Chem. Soc. Rev.* **2009**, *38*, 1294–1314. (b) Li, J. R.; Ma, Y. J.; McCarthy, M. C.; Sculley, J.; Yu, J. M.; Jeong, H. W.; Balbuena, P. B.; Zhou, H. C. Carbon dioxide capture-related gas adsorption and separation in metal-organic frameworks. *Coord. Chem. Rev.* **2011**, *255*, 1791–1823.

(6) (a) Lin, R. B.; Li, F.; Liu, S. Y.; Qi, X. L.; Zhang, J. P.; Chen, X. M. A noble-metal-free porous coordination framework with exceptional sensing efficiency for oxygen. *Angew. Chem., Int. Ed.* **2013**, *52*, 13429–13433. (b) Lustig, W. P.; Mukherjee, S.; Rudd, N. D.; Desai, A. V.; Li, J.; Ghosh, S. K. Metal-organic frameworks: functional luminescent and photonic materials for sensing applications. *Chem. Soc. Rev.* **2017**, *46*, 3242–3285. (c) DeCoste, J. B.; Peterson, G. W. Metal-organic frameworks for air purification of toxic chemicals. *Chem. Rev.* **2014**, *114*, 5695–5727.

(7) (a) Chen, Q.; Lin, J. B.; Xue, W.; Zeng, M. H.; Chen, X. M. A porous coordination polymer assembled from 8-connected $\{Co^{II}_3(OH)\}$ clusters and isonicotinate: multiple active metal sites, apical ligand substitution, H₂ adsorption, and magnetism. *Inorg. Chem.* **2011**, *50*, 2321–2328. (b) Zhou, Y. L.; Wu, M. C.; Zeng, M. H.; Liang, H. Magneto-structural correlation in a metamagnetic cobalt(II)-based pillared trilayer motif constructed by mixed pyridyl-type carboxylate ligands. *Inorg. Chem.* **2009**, *48*, 10146–10150. (c) Solea, A. B.; Wohlhauser, T.; Abbasi, P.; Mongbanziama, Y.; Crochet, A.; Fromm, K. M.; Novitchi, G.; Train, C.; Pilkington, M.; Mamula, O. Versatile synthesis of chiral 6-oxoverdazyl radical ligands—new building blocks for multifunctional molecule-based magnets. *Dalton Trans.* **2018**, *47*, 4785–4789.

(8) Zeng, M. H.; Wang, Q. X.; Tan, Y. X.; Hu, S.; Zhao, H. X.; Long, L. S.; Kurmoo, M. Rigid pillars and double walls in a porous metal-organic framework: single-crystal to single-crystal, controlled uptake and release of iodine and electrical conductivity. *J. Am. Chem. Soc.* **2010**, *132*, 2561–2563.

(9) Xu, M.; Yuan, S.; Chen, X. Y.; Chang, Y. J.; Day, G.; Gu, Z. Y.; Zhou, H. C. Two-dimensional metal-organic framework nanosheets as an enzyme inhibitor: modulation of the α -chymotrypsin activity. *J. Am. Chem. Soc.* **2017**, *139*, 8312–8319.

(10) (a) Restrepo, J.; Serroukh, Z.; Santiago-Morales, J.; Aguado, S.; Gómez-Sal, P.; Mosquera, M. E. G.; Rosal, R. An antibacterial Zn-MOF with hydrazinebenzoate linkers. *Eur. J. Inorg. Chem.* **2017**, 574–580. (b) Vasylevskiy, S. L.; Regeta, K.; Ruggi, A.; Petoud, S.; Piguet, C.; Fromm, K. M. Cis- and trans-9,10-di(1H-imidazol-1-yl)-anthracene based coordination polymers of Zn^{II} and Cd^{II}: synthesis, crystal structures and luminescence properties. *Dalton Trans.* **2018**, *47*, 596–607. (c) Lu, K. D.; Aung, T.; Guo, N. N.; Weichselbaum, R.

Lin, W. B. Nanoscale metal-organic frameworks for therapeutic, imaging, and sensing applications. *Adv. Mater.* **2018**, *30*, 1707634.

(11) (a) Loukopoulos, E.; Kostakis, G. E. Recent advances of one-dimensional coordination polymers as catalysts. *J. Coord. Chem.* **2018**, *71*, 371–410. (b) Zhang, T.; Lin, W. B. Metal-organic frameworks for artificial photosynthesis and photocatalysis. *Chem. Soc. Rev.* **2014**, *43*, 5982–5993. (c) Wen, M. C.; Mori, K.; Kuwahara, Y.; An, T. C.; Yamashita, H. Design and architecture of metal organic frameworks for visible light enhanced hydrogen production. *Appl. Catal., B* **2017**, *218*, 555–569.

(12) (a) Castro, K.; Rodrigues, R.; Mendes, R. F.; Neves, M.; Simoes, M.; Cavaleiro, J. A. S.; Almeida Paz, F. A.; Tome, J. P.; Nakagaki, S. New copper porphyrins as functional models of catechol oxidase. *J. Catal.* **2016**, *344*, 303–312. (b) Zhang, Y.; Yang, X.; Zhou, H.-C. Synthesis of MOFs for heterogeneous catalysis via linker design. *Polyhedron* **2018**, *154*, 189–201. (c) Li, C.; Tang, H.; Fang, Y.; Xiao, Z.; Wang, K.; Wu, X.; Niu, H.; Zhu, C.; Zhou, H.-c. Bottom-up assembly of a highly efficient metal-organic framework for cooperative catalysis. *Inorg. Chem.* **2018**, *57*, 13912–13919.

(13) (a) Mantovani, K.; Molgero Westrup, K. C.; da Silva, R. M.; Jaeger, S.; Wypych, F.; Nakagaki, S. Oxidation catalyst obtained by the immobilization of layered double hydroxide/Mn(III) porphyrin on monodispersed silica spheres. *Dalton Trans.* **2018**, *47*, 3068–3073.

(b) Li, G. D.; Zhao, S. L.; Zhang, Y.; Tang, Z. Y. Metal-organic frameworks encapsulating active nanoparticles as emerging composites for catalysis: recent progress and perspectives. *Adv. Mater.* **2018**, *30*, 1800702. (c) Sotnik, S. A.; Polunin, R. A.; Kiskin, M. A.; Kirillov, A. M.; Dorofeeva, V. N.; Gavrilenko, K. S.; Eremenko, I. L.; Novotortsev, V. M.; Kolotilov, S. V. Heterometallic Coordination Polymers Assembled from Trigonal Trinuclear Fe₂Ni-Pivalate Blocks and Polypyridine Spacers: Topological Diversity, Sorption, and Catalytic Properties. *Inorg. Chem.* **2015**, *54*, 5169–5181.

(14) (a) Zhao, M. T.; Yuan, K.; Wang, Y.; Li, G. D.; Guo, J.; Gu, L.; Hu, W. P.; Zhao, H. J.; Tang, Z. Y. Metal-organic frameworks as selectivity regulators for hydrogenation reactions. *Nature* **2016**, *539*, 76–80. (b) Kang, Y. S.; Lu, Y.; Chen, K.; Zhao, Y.; Wang, P.; Sun, W. Y. Metal-organic frameworks with catalytic centers: from synthesis to catalytic application. *Coord. Chem. Rev.* **2019**, *378*, 262–280.

(15) (a) Song, Z. X.; Cheng, N. C.; Lushington, A.; Sun, X. L. Recent progress on MOF-derived nanomaterials as advanced electrocatalysts in fuel cells. *Catalysts* **2016**, *6*, 116–134.

(b) Huang, N.; Drake, H.; Li, J.; Pang, J.; Wang, Y.; Yuan, S.; Wang, Q.; Cai, P. Y.; Qin, J. S.; Zhou, H. C. Flexible and hierarchical metal-organic framework composites for high-performance catalysis. *Angew. Chem., Int. Ed.* **2018**, *57*, 8916–8920. (c) Kumar, G.; Das, S. K. Coordination frameworks containing compounds as catalysts. *Inorg. Chem. Front.* **2017**, *4*, 202–233.

(16) Lu, X. B.; Darensbourg, D. J. Cobalt catalysts for the coupling of CO₂ and epoxides to provide polycarbonates and cyclic carbonates. *Chem. Soc. Rev.* **2012**, *41*, 1462–1484.

(17) Chen, X. X.; Ren, J. T.; Xie, H.; Sun, W.; Sun, M.; Wu, B. Cobalt(III)-catalyzed 1,4-addition of C–H bonds of oximes to maleimides. *Org. Chem. Front.* **2018**, *5*, 184–188.

(18) Bagherzadeh, M.; Ashouri, F.; Đaković, M. Synthesis, characterizations and catalytic studies of a new two-dimensional metal-organic framework based on Co-carboxylate secondary building units. *J. Solid State Chem.* **2015**, *223*, 32–37.

(19) Qin, L.; Lu, K.; Li, X.; Yan, J. J.; Lin, W. J.; Ding, W. Q.; Lu, H.; Lin, D. T.; Ma, D. Y.; Liang, F. L. Unusual 1D tape of pentameric and tetrameric water clusters trapped in a 2D cobalt(II) coordination polymer: synthesis, characterization, and catalytic properties. *J. Inorg. Organomet. Polym. Mater.* **2016**, *26*, 460–466.

(20) Wang, F. Artificial photosynthetic systems for CO₂ reduction: progress on higher efficiency with cobalt complexes as catalysts. *ChemSusChem* **2017**, *10*, 4393–4402.

(21) Kornienko, N.; Zhao, Y. B.; Kley, C. S.; Zhu, C. H.; Kim, D.; Lin, S.; Chang, C. J.; Yaghi, O. M.; Yang, P. D. Metal-organic frameworks for electrocatalytic reduction of carbon dioxide. *J. Am. Chem. Soc.* **2015**, *137*, 14129–14135.

(22) Kramer, W. W.; McCrory, C. C. L. Polymer coordination promotes selective CO₂ reduction by cobalt phthalocyanine. *Chem. Sci.* **2016**, *7*, 2506–2515.

(23) Xu, H. W.; Williard, P. G.; Bernskoetter, W. H. C–H bond activation and S-atom transfer from cobalt(III) thiolate and isothiocyanate complexes. *Dalton Trans.* **2014**, *43*, 14696–14700.

(24) Hazra, S.; Pilania, P.; Deb, M.; Kushawaha, A. K.; Elias, A. J. Aerobic Oxidation of Primary Amines to Imines in Water using a Cobalt Complex as Recyclable Catalyst under Mild Conditions. *Chem. - Eur. J.* **2018**, *24*, 15766–15771.

(25) Chakrabarty, R.; Bora, S. J.; Das, B. K. Synthesis, Structure, Spectral and Electrochemical Properties, and Catalytic Use of Cobalt(III)-Oxo Cubane Clusters. *Inorg. Chem.* **2007**, *46*, 9450–9462.

(26) Kharat, A. N.; Bakhoda, A.; Jahromi, B. T. Green and chemoselective oxidation of alcohols with hydrogen peroxide: A comparative study on Co(II) and Co(III) activity toward oxidation of alcohols. *Polyhedron* **2011**, *30*, 2768–2775.

(27) Gu, J. Z.; Liang, X. X.; Cai, Y.; Wu, J.; Shi, Z. F.; Kirillov, A. M. Hydrothermal assembly, structures, topologies, luminescence, and magnetism of a novel series of coordination polymers driven by a trifunctional nicotinic acid building block. *Dalton Trans.* **2017**, *46*, 10908–10925.

(28) Gu, J. Z.; Cui, Y. H.; Liang, X. X.; Wu, J.; Lv, D. Y.; Kirillov, A. M. Structurally distinct metal-organic and H-bonded networks derived from 5-(6-carboxypyridin-3-yl)isophthalic acid: coordination and template effect of 4,4'-bipyridine. *Cryst. Growth Des.* **2016**, *16*, 4658–4670.

(29) (a) Gu, J. Z.; Cai, Y.; Qian, Z. Y.; Wen, M.; Shi, Z. F.; Lv, D. Y.; Kirillov, A. M. A new series of Co, Ni, Zn, and Cd metal-organic architectures driven by an unsymmetrical biphenyl-tricarboxylic acid: hydrothermal assembly, structural features and properties. *Dalton Trans.* **2018**, *47*, 7431–7444. (b) Gu, J. Z.; Wen, M.; Liang, X.; Shi, Z.-F.; Kirillova, M. V.; Kirillov, A. M. Multifunctional Aromatic Carboxylic Acids as Versatile Building Blocks for Hydrothermal Design of Coordination Polymers. *Crystals* **2018**, *8*, 83.

(30) Gu, J. Z.; Cai, Y.; Wen, M.; Shi, Z. F.; Kirillov, A. M. A new series of Cd(II) metal-organic architectures driven by soft ether-bridged tricarboxylate spacers: synthesis, structural and topological versatility, and photocatalytic properties. *Dalton Trans.* **2018**, *47*, 14327–14339.

(31) (a) Fernandes, T. A.; Santos, C. I. M.; André, V.; Klak, J.; Kirillova, M. V.; Kirillov, A. M. Copper(II) Coordination Polymers Self-assembled from Aminoalcohols and Pyromellitic Acid: Highly Active Pre-catalysts for the Mild Water-promoted Oxidation of Alkanes. *Inorg. Chem.* **2016**, *55*, 125–135. (b) Dias, S. S. P.; Kirillova, M. V.; André, V.; Klak, J.; Kirillov, A. M. New tricopper(II) cores self-assembled from aminoalcohol biobuffers and homophthalic acid: synthesis, structural and topological features, magnetic properties and mild catalytic oxidation of cyclic and linear C5–C8 alkanes. *Inorg. Chem. Front.* **2015**, *2*, 525–537. (c) Kirillova, M. V.; Kirillov, A. M.; Kuznetsov, M. L.; Silva, J. A. L.; Fraústo da Silva, J. J. R.; Pombeiro, A. J. L. Alkanes to carboxylic acids in aqueous medium: metal-free and metal-promoted highly efficient and mild conversions. *Chem. Commun.* **2009**, 2353–2355.

(32) Śliwa, E. I.; Nesterov, D. S.; Klak, J.; Jakimowicz, P.; Kirillov, A. M.; Smoleński, P. Unique Copper-Organic Networks Self-Assembled from 1,3,5-Triaza-7-Phosphaadamantane and its Oxide: Synthesis, Structural Features, Magnetic and Catalytic Properties. *Cryst. Growth Des.* **2018**, *18*, 2814–2823.

(33) (a) Nesterov, D. S.; Nesterova, O. V. Polynuclear Cobalt Complexes as Catalysts for Light-Driven Water Oxidation: A Review of Recent Advances. *Catalysts* **2018**, *8*, 602. (b) Nesterova, O. V.; Kopylovich, M. N.; Nesterov, D. S. Stereoselective oxidation of alkanes with m-CPBA as an oxidant and cobalt complex with isoindole-based ligands as catalysts. *RSC Adv.* **2016**, *6*, 93756–93767.

(34) Zheng, X. B.; Fan, R. Q.; Song, Y.; Wang, A.; Xing, K.; Du, X.; Wang, P.; Yang, Y. L. A highly sensitive turn-on ratiometric

luminescent probe based on postsynthetic modification of $\text{Tb}^{3+}@\text{Cu-MOF}$ for H_2S detection. *J. Mater. Chem. C* **2017**, *5*, 9943–9951.

(35) Xue, L.-P.; Shan, L.-L.; Feng, W.-J. Synthesis, crystal structure and luminescence of a cadmium(II) coordination polymer with 3,6-connected rtl topology. *Chin. J. Struct. Chem.* **2016**, *35*, 293–297.

(36) Liu, Y. L.; Chen, F. Y.; Di, Y. Q.; Cao, J.; Di, Y. L.; Zhou, C. S. Two coordination polymers based on a flexible tritopic pyridyldicarboxylate ligand: structures and magnetic properties. *Z. Anorg. Allg. Chem.* **2016**, *642*, 246–249.

(37) Wu, W. P.; Li, Z. S.; Liu, B.; Liu, P.; Xi, Z. P.; Wang, Y. Y. Double-step CO_2 sorption and guest-induced single-crystal-to-single-crystal transformation in a flexible porous framework. *Dalton Trans.* **2015**, *44*, 10141–10145.

(38) Gu, J. Z.; Cai, Y.; Liang, X. X.; Wu, J.; Shi, Z. F.; Kirillov, A. M. Bringing 5-(3,4-dicarboxylphenyl)picolinic acid to crystal engineering research: hydrothermal assembly, structural features, and photocatalytic activity of Mn, Ni, Cu, and Zn coordination polymers. *CrystEngComm* **2018**, *20*, 906–916.

(39) Li, Y.; Zou, X. Z.; Gu, J. Z.; Cheng, X. L. Syntheses, crystal structures and magnetic properties of two copper(II) and manganese(II) coordination compounds constructed from biphenyl tricarboxylic acid. *Chin. J. Inorg. Chem.* **2018**, *34*, 1159–1165.

(40) (a) Sheldrick, G. M. A program for automatic solution of crystal structure. *Acta Crystallogr., Sect. A: Found. Crystallogr.* **1990**, *A46*, 467–473. (b) Sheldrick, G. M. *SHELXS-97: A Program for X-ray Crystal Structure Solution, and SHELXL-97: A Program for X-ray Structure Refinement*; University of Göttingen: Göttingen, Germany, 1997.

(41) Shul'pin, G. B. Metal-catalyzed hydrocarbon oxygenations in solutions: The dramatic role of additives: a review. *J. Mol. Catal. A: Chem.* **2002**, *189*, 39–66.

(42) (a) Shul'pin, G. B. New Trends in Oxidative Functionalization of Carbon-Hydrogen Bonds: A Review. *Catalysts* **2016**, *6*, 50.

(b) Shul'pin, G. B. Selectivity enhancement in functionalization of C-H bonds: A review. *Org. Biomol. Chem.* **2010**, *8*, 4217–4228.

(43) (a) Blatov, V. A. Multipurpose crystallochemical analysis with the program package TOPOS. *Compcomm. Newsl.* **2006**, No. 7, 4–38.

(b) Blatov, V. A.; Shevchenko, A. P.; Proserpio, D. M. Applied topological analysis of crystal structures with the program package topospro. *Cryst. Growth Des.* **2014**, *14*, 3576–3586.

(44) (a) O'Keeffe, M.; Yaghi, O. M. Deconstructing the crystal structures of metal-organic frameworks and related materials into their underlying nets. *Chem. Rev.* **2012**, *112*, 675–702. (b) Li, M.; Li, D.; O'Keeffe, M.; Yaghi, O. M. Topological analysis of metal-organic frameworks with polytopic linkers and/or multiple building units and the minimal transitivity principle. *Chem. Rev.* **2014**, *114*, 1343–1370.

(45) O'Keeffe, M.; Peskov, M. A.; Ramsden, S. J.; Yaghi, O. M. The reticular chemistry structure resource (RCSR) database of, and symbols for, crystal nets. *Acc. Chem. Res.* **2008**, *41*, 1782–1789.

(46) See the Cambridge Structural Database (CSD, 2018). Groom, C. R.; Bruno, I. G.; Lightfoot, M. P.; Ward, S. C. The Cambridge structural database. *Acta Crystallogr., Sect. B: Struct. Sci., Cryst. Eng. Mater.* **2016**, *B72*, 171–179.

(47) (a) Miranda, J. F.; Zapata, P. M. C.; Gonzo, E. E.; Parentis, M. L.; Davies, L. E.; Bonini, N. A. Amorphous Cr/SiO₂ Materials Hydrothermally Treated: Liquid Phase Cyclohexanol Oxidation. *Catal. Lett.* **2018**, *148*, 2082–2094. (b) Narayanan, S.; Vijaya, J. J.; Sivasanker, S.; Alam, M.; Tamizhdurai, P.; Kennedy, L. J. Characterization and catalytic reactivity of mordenite – Investigation of selective oxidation of benzyl alcohol. *Polyhedron* **2015**, *89*, 289–296.

(48) (a) Gogoi, N.; Begum, T.; Dutta, S.; Bora, U.; Gogoi, P. K. Rice husk derived nanosilica supported Cu(II) complex: an efficient heterogeneous catalyst for oxidation of alcohols using TBHP. *RSC Adv.* **2015**, *5*, 95344–95352. (b) Burange, A. S.; Jayaram, R. V.; Shukla, R.; Tyagi, A. K. Oxidation of benzylic alcohols to carbonyls using tert-butyl hydroperoxide over pure phase nanocrystalline CeCrO₃. *Catal. Commun.* **2013**, *40*, 27–31.

(49) Fan, Y.; Li, X.; Gao, K.; Liu, Y.; Meng, X.; Wu, J.; Hou, H. Co(II)-cluster-based metal-organic frameworks as efficient hetero-

geneous catalysts for selective oxidation of arylalkanes. *CrystEngComm* **2019**, *21*, 1666–1673.

(50) Farrokhi, A.; Jafarpour, M.; Najafzade, R. Phosphonate-based Metal Organic Frameworks as Robust Heterogeneous Catalysts for TBHP Oxidation of Benzylic Alcohols. *Catal. Lett.* **2017**, *147*, 1714–1721.